PLOS PATHOGENS

Picornavirus security proteins promote the release of extracellular vesicle enclosed viruses via the modulation of host kinases

Kyra A. Y. Defourny[1], Xinyi Pei[1], Frank J. M. van Kuppeveld[2], Esther N. M. Nolte-´t Hoen [1]*

1 Infection Biology Section, Division of Infectious Diseases & Immunology, Department of Biomolecular Health Sciences, Faculty of Veterinary Medicine, Utrecht University, Utrecht, The Netherlands, 2 Virology Section, Division of Infectious Diseases & Immunology, Department of Biomolecular Health Sciences, Faculty of Veterinary Medicine, Utrecht University, Utrecht, The Netherlands

* e.n.m.nolte@uu.nl

Abstract

The discovery that extracellular vesicles (EVs) serve as carriers of virus particles calls for a reevaluation of the release strategies of non-enveloped viruses. Little is currently known about the molecular mechanisms that determine the release and composition of EVs produced by virus-infected cells, as well as conservation of these mechanisms among viruses. We previously described an important role for the Leader protein of the picornavirus encephalomyocarditis virus (EMCV) in the induction of virus-carrying EV subsets with distinct molecular and physical properties. EMCV L acts as a 'viral security protein' by suppressing host antiviral stress and type-I interferon (IFN) responses. Here, we tested the ability of functionally related picornavirus proteins of Theilers murine encephalitis virus (TMEV L), Saffold virus (SAFV L), and coxsackievirus B3 (CVB3 $2A^{pro}$), to rescue EV and EV-enclosed virus release when introduced in Leader-deficient EMCV. We show that all viral security proteins tested were able to promote virus packaging in EVs, but that only the expression of EMCV L and CVB3 $2A^{pro}$ increased overall EV production. We provide evidence that one of the main antiviral pathways counteracted by this class of picornaviral proteins, i.e. the inhibition of PKR-mediated stress responses, affected EV and EV-enclosed virus release during infection. Moreover, we show that the enhanced capacity of the viral proteins EMCV L and CVB3 $2A^{pro}$ to promote EV-enclosed virus release is linked to their ability to simultaneously promote the activation of the stress kinase P38 MAPK. Taken together, we demonstrate that cellular stress pathways involving the kinases PKR and P38 are modulated by the activity of non-structural viral proteins to increase the release EV-enclosed viruses during picornavirus infections. These data shed new light on the molecular regulation of EV production in response to virus infection.

analysis, decision to publish, or preparation of the manuscript.

Author summary

During infection, virus particles can be packaged by host cells within extracellular vesicles (EVs), nanosized vesicles that serve as vehicles for cell-to-cell communication. These EVs can shield virus particles from antibodies, and alter the uptake of viruses by susceptible cells and cells carrying-out immune surveillance. However, despite the potential consequences of EV-enclosed virus release on disease progression, little is known about the virus and host factors regulating this process. Here, we investigated the role of virus-encoded host-modulating proteins in the packaging of non-enveloped viruses in EVs, focusing on the *picornavirus* virus family. We previously demonstrated that the picornavirus encephalomyocarditis virus alters the number and type of EVs released by infected cells to promote EV-enclosed virus release, and that this depended on the activity of the viral Leader protein. Using a panel of knockout cells, inhibitors, and recombinant virus constructs, we here show that this alteration of EV release depends on modulation of the pathways downstream of two host stress kinases, PKR and P38 MAPK, and is conserved in the 2A protease of distantly related pathogen coxsackievirus B3. These data shed light on the molecular regulation of EV-enclosed virus release, and pave the way to find inhibitors of EV-mediated virus spread.

Introduction

A growing number of non-enveloped viruses are known to be released from infected cells in two forms: as naked virions, and as quasi-enveloped virus particles enclosed in host-derived membranes. In contrast to enveloped viruses, non-enveloped viruses lack specialized transmembrane proteins to induce membrane budding and release. Instead, these viruses make use of the host's natural ability to produce membrane vesicles, also known as extracellular vesicles or EVs, to induce the release of virions in a membrane-enclosed form. EVs are naturally released by all cells as a means of cell-to-cell communication [1]. Whereas the release of naked virions typically requires lysis of the host cell, the packaging of virions within EVs allows viruses to escape the host cell prior to the rupture of cellular membranes [2–5]. This process results in the formation of infectious virus particles that differ in functional properties compared to their naked counterparts. Depending on the exact composition of the EV carrier, including the number of enclosed virus particles, EV-enclosed viruses can display altered uptake and infection dynamics [6–12]. Importantly, EV-enclosed virus particles become inaccessible for neutralizing antibodies [13–17]. Hence, EVs constitute long overlooked players in the viral life cycle as well as a determinant of infection progression.

 Initial studies have provided first insight into how the release of EV-enclosed virus is regulated. Although virions may be packaged in EVs that are constitutively released by cells, many viruses were found to alter EV release by the host cell. The non-enveloped viruses encephalomyocarditis virus (EMCV), rotavirus, astrovirus, enterovirus A71, and hepatitis A virus (HAV) were shown to increase EV production during infection [4,18–21]. Moreover, we previously demonstrated that EMCV infection induced the release of specific EV subsets with distinct protein composition, physical properties, and potential to infect cells [4]. For HAV, EV-enclosed virus release was shown to be promoted by an interaction between the EV biogenesis protein Alix and a motif within the viral capsid [20]. In contrast, for other members of the family *Picornaviridae*, most notably EMCV, poliovirus, and coxsackievirus B3 (CVB3), the autophagy machinery has been implicated in the packaging of virions in EVs [2,22–25]. These viruses trigger an unconventional arm of the autophagy pathway, termed secretory autophagy,

via which autophagosomal cargo is delivered to the extracellular environment instead of the lysosomal degradation pathway [26]. We previously demonstrated that the ability of EMCV to induce secretory autophagy as well as the release of EVs and EV-enclosed virus required the expression of the non-structural viral Leader (L) protein [25]. However, the mechanisms via which EMCV L, and possibly also non-structural proteins of other picornaviruses, modulate host cells to enable the release of virus-containing EVs are unknown.

EMCV L is a multifunctional protein that is dispensable for virus replication but is key to altering host cell signaling and function during infection [27]. The activity of EMCV L is crucial for the suppression of type-I interferon induction, which is primarily mediated by the disruption of the nucleopore complex resulting in nucleocytoplasmic trafficking disorder (NCTD) [28]. In addition, EMCV L suppresses the integrated cellular stress response and formation of stress granules during infection [29,30]. To mediate these effects, EMCV L directly or indirectly modulates the activity of host cell kinases [31–34]. Notably, non-structural proteins of many other picornaviruses have evolved to target similar host processes via diverse molecular mechanisms, despite sharing little to no overlap in sequence or structure. These evolutionary heterogenous picornaviral proteins have previously been referred to as "viral security proteins", based on their shared functions in counteracting host-defense mechanisms [35]. The security proteins that share most overlap with EMCV L (±40% amino acid similarity), are the L proteins of Theiler's murine encephalitis virus (TMEV) and Saffold virus (SAFV), which together with EMCV form the genus *Cardiovirus* within the *Picornaviridae* [36]. The cardiovirus L proteins were previously reported to be functionally interchangeable, as EMCV L was able to modulate host defense and induce NCTD when replacing TMEV L in the TMEV genome [29,37,38]. The same functional interchangeability has been demonstrated for more distant picornavirus security proteins, as the 2A protease (2A^{pro}) of the enterovirus CVB3 was able to suppress stress granule formation and IFN induction when exchanged with EMCV L, despite the lack of similarity in sequence or structure of these proteins [38].

In this study, we first investigated whether different picornavirus non-structural proteins that are known to subvert the same cellular defense mechanisms also share the ability to promote the release of EV-enclosed viruses. In our comparison we included EMCV L, TMEV L, SAFV L, and CVB3 2A^{pro}, which all suppress SG formation and type I IFN production while inducing NCTD. The ability of TMEV L, SAFV L, and CVB3 2A^{pro} to promote EV-enclosed virus release was tested using a recombinant virus system in which we inserted these viral proteins into an EMCV strain lacking L protein activity. We show that all tested proteins could promote the release of EV-enclosed EMCV, but with different efficiencies. Only EMCV L and CVB3 2A^{pro} could trigger alterations in the number and composition of EVs released by infected cells and induced the release of a distinct virus-carrying EV subset. We subsequently made use of the functional commonalities and differences between these viral security proteins to identify host processes and signaling pathways that affect the release of EV-enclosed viruses. Using knockout and chemical inhibition strategies, we demonstrate a role for PKR and P38 MAPK signaling pathways in determining the efficiency with which EV-enclosed viruses are released in response to virus infection.

Results

The activities of picornavirus security proteins EMCV L, TMEV L, SAFV L, and CVB3 2A^{pro} promote EV-enclosed virus release

We previously showed that EMCV L plays an important role in the release of virus-carrying EV subsets during EMCV infection [25]. To investigate whether this function is shared among security proteins of related picornaviruses, we employed a recombinant virus system in which

different viral security proteins could be expressed in the context of the EMCV genome. In this system, genes encoding the L proteins of the cardioviruses TMEV and SAFV, as well as the 2A^{pro} protein of the enterovirus CVB3, were inserted into the genome of mutant EMCV carrying an inactivating mutation in its own L protein (EMCV-L^{Zn}) (Fig 1A). EMCV-L^{Zn} is unable to suppress PKR activation and downstream stress granule formation, and fails to induce NCTD to suppress IFN-β production, thereby allowing the activation of these two important antiviral pathways during infection [30,39]. As anticipated, we observed that insertion of TMEV L (EMCV-L^{TMEV}), SAFV L (EMCV-L^{SAFV}), and CVB3 2A^{pro} (EMCV-2A^{pro}) could restore the capacity of EMCV-L^{Zn} to modulate these host defense processes (S1 Fig) [28,35]. Notably, whereas the three Leader proteins directly inhibit PKR activation, we confirmed that CVB3 2A^{pro} suppresses the PKR antiviral pathway downstream of PKR (S1 Fig). The replication kinetics of recombinant EMCV-L^{Zn} viruses expressing TMEV L, SAFV L or CVB3 2A^{pro} were similar to EMCV-L^{Zn} (Fig 1B), as no significant difference in virus yields could be observed at any of the time points tested. However, intracellular virus titers for EMCV-Wt were significantly higher than for the other viruses from 7 hpi onwards (Fig 1C). We used EMCV-Wt and these recombinant viruses to investigate whether TMEV L, SAFV L, and CVB3 2A^{pro} share with EMCV L the ability to promote EV-enclosed virus release, and to determine if known functions ascribed to these proteins are important for this process.

We first assessed whether expression of the different picornavirus security proteins influenced total extracellular virus release. Expression of functional EMCV L (EMCV-Wt) or CVB3 2A^{pro} (EMCV-2A^{pro}) significantly increased EMCV virus release compared to that observed for EMCV-L^{Zn} starting at 7 hpi (Fig 1D and 1E). EMCV L and CVB3 2A^{pro} proteins were found to increase virus release with a similar efficiency when values were corrected for the respective differences in intracellular virus titers (S2 Fig). In contrast, expression of TMEV L and SAFV L increased virus release to a lesser extent and only from 9–10 hpi (Fig 1D and 1E). This increase in virus release preceded a strong increase in the permeability of the infected cells, which occurred at 8 hpi for EMCV-Wt and EMCV-2A^{pro} infected cells and at 11 hpi for EMCV-L$^{TMEV/SAFV}$ infected cells (S3 Fig). To assess if the increase in overall virus release observed at these time points correlated with an increase in the release of EV-enclosed virus, EVs were isolated from the cell culture supernatant of infected cells and separated from naked virions using density gradient centrifugation as described previously [4]. EMCV-Wt and EMCV-2A^{pro} induced a significant increase in EV-enclosed virus release at 7 hpi compared to EMCV-L^{Zn} (Fig 1F). This effect was larger for EMCV-Wt, in correspondence with the higher intracellular virus titers in EMCV-Wt infected cells (Fig 1C). At 10 hpi also the incorporation of TMEV L and SAFV L in EMCV-L^{Zn} enhanced EV-enclosed virus release, although to a lesser extent than observed for CVB3 2A^{pro} at 7 hpi (Fig 1F). In contrast to the cardiovirus leaders, CVB3 2A^{pro} is a viral protease. Both protease-dependent and independent functions have been attributed to the enterovirus 2A protein [38,40–42]. Mutation of the catalytic domain of CVB3 2A^{pro} did not affect intracellular virus titers (S4A Fig), but abolished its positive effect on EV-enclosed virus release, indicating that the ability of CVB3 2A^{pro} to promote EV-enclosed virus release required its proteolytic activity (Fig 1G). Based on these data, we conclude that the viral security proteins TMEV L, SAFV L, and CVB3 2A^{pro} are all able to promote EV-enclosed virus release during EMCV infection. Notably, the impact of TMEV L and SAFV L on EV-enclosed virus release was delayed and less pronounced (4.6 and 5.4 mean fold increase at T = 10) compared to that of proteolytic active CVB3 2A^{pro} (67.6 mean fold increase at T = 7) or EMCV L (2691.5 mean fold increase at T = 7, with an accompanying 23.3 fold increase in intracellular virus).
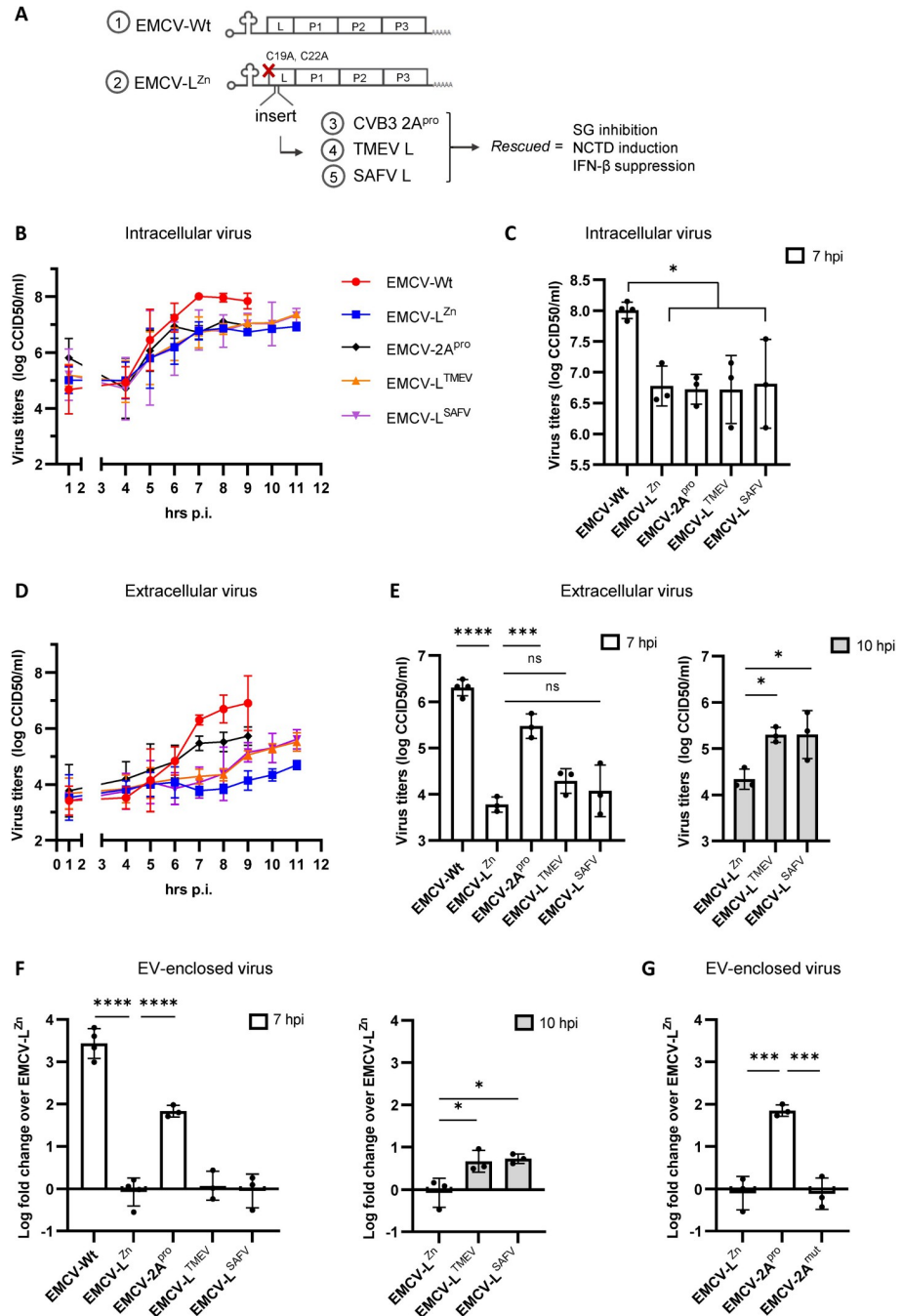
Fig 1. The picornavirus security proteins CVB3 2A^{Pro}, TMEV L, and SAFV L promote EV-enclosed virus release with different efficiencies. (A) Depicted is a schematic overview of the recombinant viruses used in this study. To generate these viruses, the coding sequences of TMEV L (L^{TMEV}), SAFV L (L^{SAFV}), or CVB3 2A (2A^{pro}) proteins were fused to the polyprotein of an EMCV strain containing an inactivating mutation in the EMCV L protein (EMCV-L^{Zn}), separated by a 3C cleavage site. (B-G) HeLa cells were infected with the viruses described in (A) at MOI 10. (B) Intracellular virus titers were determined over time by end-point dilution assay and are depicted as line graph. In (C) a bar graph is depicted comparing the intracellular virus titers at 7 hpi. Corresponding extracellular virus titers are depicted in (D) and (C), with bar graphs comparing the extracellular virus titers at 7 hpi (left) and 10 hpi (right). (F) EVs released by cells infected with EMCV-Wt, EMCV-L^{Zn}, or EMCV-L^{Zn} reconstituted with the indicated viral proteins were isolated by density gradient centrifugation at 7 or 10 hpi. EV-enclosed virus titers were determined by end-point dilution assay. Data are expressed as fold increase in EV-enclosed virus titers relative to EMCV-L^{Zn}. (G) EV-enclosed virus release at 7 hpi was compared for EMCV-L^{Zn} reconstituted with proteolytically active *vs.* proteolytically inactive CVB3 2A^{pro} (EMCV-2A^{pro} and EMCV-2A^{mut} respectively). Bar and line graphs depict means ± SD of n = 3–4

independent experiments. *p<0.05, ***p<0.0005, ****p<0.0001 as determined by one-way ANOVA with Tukey's multiple comparisons test.

The activities of EMCV L and CVB3 2A^{pro}, but not TMEV L or SAFV L, increase the release of distinct EV subsets during infection

Based on the differences observed in EV-enclosed virus release, we next set out to study the impact of the different viral security proteins on the number and type of EVs released by the infected cells. We applied high-resolution flow cytometry to analyze the quantity and quality of EVs released during infection at a single particle level [4,43,44]. Using this technique, we observed a 5- to 10-fold increase in the number of released EVs upon infection with EMCV-2A^{pro}, which is similar to the induction of EV release observed during EMCV-Wt infection (Fig 2A). In line with our observations on EV-enclosed virus release (Fig 1E), the impact of CVB3 2A^{pro} on EV release was dependent on its protease activity (S4B Fig). However, expression of TMEV L or SAFV L did not restore induction of EV release by EMCV-L^{Zn} infected cells at 7 or 10 hpi (Fig 2A). In EV isolates from EMCV-Wt and EMCV-2A^{pro} infected cells, two EV populations were observed that induced different levels of forward scattered light (FSC) (Fig 2B). Our previous data indicate that FSC-high EVs contribute most to the spread of EMCV infection to new cells [4]. An increase in the percentage of FSC-high EVs was observed during infection with EMCV-Wt and EMCV-2A^{pro}, but not with TMEV L or SAFV L expressing recombinant viruses (Fig 2C). This suggests that the activity of EMCV L and CVB3 2A^{pro}, but not the other cardiovirus L proteins, can promote the release of distinct EV subsets in response to EMCV infection.

Western blot was performed to compare the protein composition of the EVs released by cells infected with the different viruses. Infection with EMCV-2A^{pro} enhanced the release of EVs carrying the tetraspanin CD9 and flotillin, resembling the EV subpopulation(s) induced by EMCV-Wt infection (Fig 2D). Moreover, LC3 could be detected in the EVs from cells infected with EMCV-Wt or EMCV-2A^{pro}. More specifically, we detected a band corresponding to LC3-II, the lipidated form of LC3 (S5 Fig). LC3 is an autophagy-related protein, and its incorporation in EV marks the activation of a secretory arm of the autophagy pathway that we previously linked to virus packaging in EVs [25]. In contrast, EMCV-L^{TMEV} and EMCV-L^{SAFV} did not prominently enhance the release of flotillin and LC3 at 7 or 10 hpi (Fig 2D), although infection with EMCV-L^{TMEV} increased the release of CD9 at 10 hpi. These data indicate that along with the rapid induction of EV-enclosed virus release, CVB3 2A^{pro} shares with EMCV L the ability to efficiently promote the release of infection-related EV subsets, which are marked by a FSC-high phenotype and the presence of flotillin and LC3-II. The activity of TMEV L or SAFV L, on the other hand, only moderately promotes virus packaging in EVs at a later stage of the infection without an accompanying increase in overall EV release. Combined, these data indicate that security proteins from various picornaviruses promote the release of EV-enclosed EMCV, but with different efficiencies. Only EMCV L and CVB3 2A^{pro} induced alterations in the number and composition of EVs released by infected cells and induced the release of a distinct virus-carrying EV subset.

Suppression of PKR activity, but not MAVS-mediated antiviral signaling, potentiates the release of EVs and EV-enclosed virus during EMCV infection

All tested viral security proteins tested share the ability to suppress SG formation and IFN-β induction. Therefore, we next investigated whether inhibition one or both of these processes

Picornavirus proteins promote release of virus via extracellular vesicles by modulating host kinases
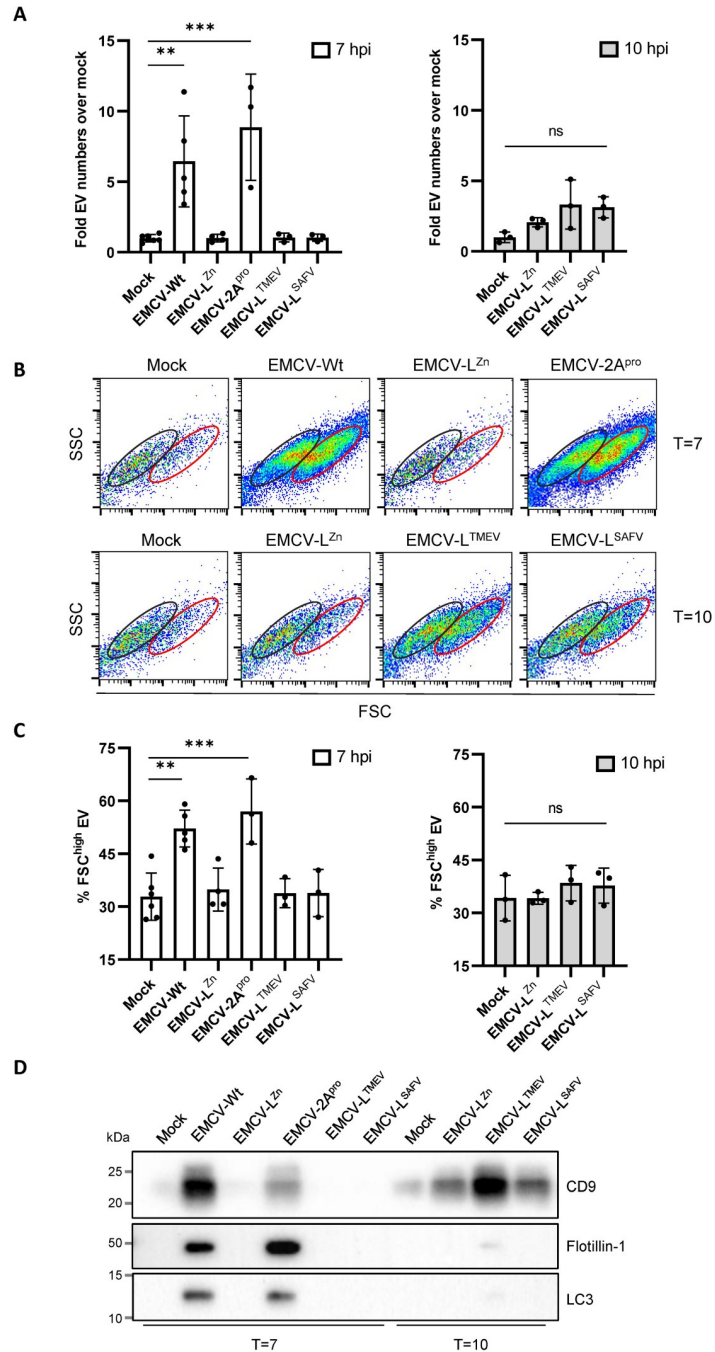
Fig 2. CVB3 2A^{pro} and EMCV L, but not TMEV L or SAFV L, strongly increase the release of virus-induced EV subsets carrying flotillin-1 and LC3. EVs were isolated by means of density gradient centrifugation at 7 or 10 hpi with EMCV-Wt, EMCV-L^{Zn}, or the recombinant viruses EMCV-2A^{pro}, EMCV-L^{TMEV}, and EMCV-L^{SAFV}. (A) EVs were fluorescently labeled with CFSE and quantified by high resolution flow cytometry. Depicted is the increase in EV numbers relative to the mock-infected control. Means ± SD of n = 3–4 independent experiments are shown. (B) Dot plots showing the forward (FSC) *vs*. side-scatter (SSC) profile of EVs in the peak fraction of samples corresponding to (A). (C) Bar graphs displaying the % of total EVs that fall within the FSC^{high} gate indicated in (B). (D) Western blot analysis of CD9, flotillin-1, and LC3 in density gradient purified EVs isolated from an equal number of cells. Depicted are representative images of n = 2 independent experiments. p**<0.005, ***p<0.0001 as determined by one-way ANOVA with Tukey's multiple comparisons test.

plays a role in potentiating EV-enclosed virus release in infected cells. Induction of IFN-β expression in response to EMCV infection requires detection of the virus by the antiviral sensor MDA-5, which subsequently activates the downstream adaptor protein MAVS [30]. In contrast, the formation of stress granules in response to EMCV infection relies on the sensing of the virus by the antiviral sensor PKR [30]. We therefore decided to use KO cell lines for the host factors MAVS and PKR to assess whether preventing the induction of these two antiviral signaling pathways during EMCV-L^{Zn} infection affects EV and EV-enclosed virus release. WT, MAVS KO, and PKR KO cells were infected with EMCV-L^{Zn} or EMCV-Wt as control, followed by comparison of intracellular and EV-enclosed virus titers. Virus titers in MAVS KO cells resembled those observed in WT cells (Fig 3A). Knock out of PKR, on the other hand, negated the difference in intracellular virus titers between EMCV-Wt and EMCV-L^{Zn} infected cells, and reduced the difference in EV-enclosed virus release (Fig 3A). Upon normalization for the potential differences in intracellular virus production, it was clear that EMCV-L^{Zn} induced less EV-enclosed virus release than EMCV-Wt in all cell lines, but that this defect was significantly reduced in PKR KO cells (Fig 3B). In line with this finding, we observed that PKR KO (partially) rescued the increase in overall EV numbers (Fig 3C) as well as the induction of the FSC-high EV subsets carrying flotillin and LC3 during EMCV-L^{Zn} infection (Figs 3D, 3E and S6A). In contrast, the number and composition of EVs released by MAVS KO cells remained comparable to that observed in WT cells upon infection with either virus (Figs 3D, 3F and S6B). These data indicate that the inhibition of the PKR antiviral signaling and downstream SG formation, but not MDA5-MAVS signaling, potentiates the release of EVs and EV-enclosed virus during EMCV infection.

Inhibition of the PKR antiviral pathway by CVB3 2A^{pro} is believed to rely on the cleavage of (unknown) host factors downstream of PKR. Yet the cardiovirus Leaders were recently described to inhibit PKR activation via physical interaction with and activation of the host kinase RSK [31]. Therefore, we assessed if the knocking out RSK would reduce the ability of EMCV-Wt to induce EV-enclosed virus release. Knock out of RSK-1-3 homologues (TKO) reduced intracellular virus titers (Fig 4A) but caused an even greater decrease in EV-enclosed virus release 7 hpi (Fig 4A, normalized data in Fig 4B). This effect could be restored by reconstitution of RSK-2 (Fig 4A and 4B). In line with these findings, high resolution flow cytometry analysis confirmed that RSK depletion abolished the increase in EV release induced by EMCV infection and that this was (partially) restored upon re-introduction of RSK-2 (Fig 4C). These data further support the notion that inhibition of the PKR antiviral pathway is required for enhanced release of EVs and EV-enclosed viruses during EMCV infection, and that for cardiovirus Leaders this relies on the interaction with the host kinase RSK.

A role for P38 MAPK in the induction of EV and EV-enclosed virus release by EMCV L and CVB3 2A^{pro}

The above data demonstrate an important role for inhibition of the PKR pathway in enabling the production of virus-carrying EV subsets. Yet, recombinant viruses expressing TMEV L or SAFV L were not able to rescue the induction of virus-induced EV subsets (Fig 2A, 2D and 2E), despite causing a similar degree of PKR inhibition as EMCV-Wt (S1A Fig). Furthermore, PKR KO did not fully restore the production of virus-carrying EVs by leader-deficient *vs*. Wt EMCV despite highly similar intracellular virus titers (Fig 3A and 3B). This suggests that viral proteins such as EMCV L modulate additional host cell pathways involved in the regulation of EV-enclosed virus release. Hence, we aimed to identify host cell pathways that were differentially regulated by the recombinant viruses EMCV-L$^{TMEV/SAFV}$ *versus* EMCV-2A^{pro}/
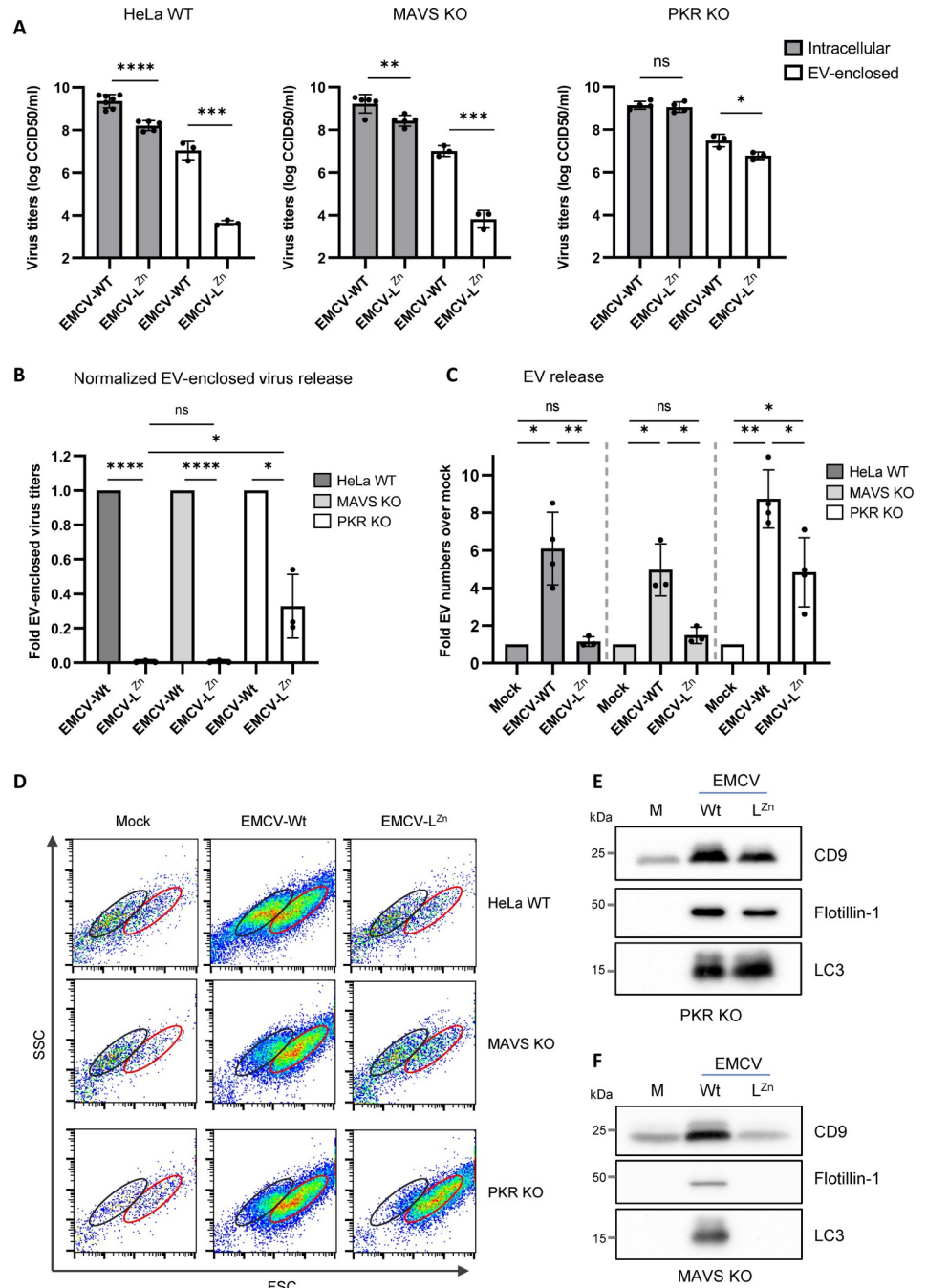
Fig 3. Suppression of PKR but not MAVS antiviral signaling potentiates the release of EVs and EV-enclosed virus during EMCV infection. WT, MAVS KO, and PKR KO cells were infected with EMCV-Wt or EMCV-L^{Zn}. 7 hpi EVs were isolated by density gradient centrifugation to assess if inhibition of MAVS/PKR-mediated antiviral signaling cascades can rescue EV-enclosed virus release. (A) Intracellular and EV-enclosed virus titers were determined by end-point dilution assay. (B) Bar graphs displaying the fold difference in EV-enclosed virus titers detected in EMCV-L^{Zn} compared to EMCV-Wt infected samples, after correction for the corresponding differences in intracellular virus titers. Means ± SD of n≥3 independent experiments are shown. (C) EV numbers were quantified by high resolution flow cytometry. Depicted is the increase in EV numbers relative to the mock-infected controls. Means ± SD of n = 4 independent experiments are shown. (D) Dot plots showing the forward (FSC) *vs.* side-scatter (SSC) profile of EVs in the peak fraction of samples corresponding to (C). (E,F) EVs isolated by ultracentrifugation from an equal number of (mock) infected MAVS (E) or PKR KO cells (F) were analyzed for the presence of the common EV-associated proteins CD9 and flotillin-1. In addition, the extracellular release of LC3 was analyzed. Representative images of n≥2 independent experiments are shown. * p<0.05, ** p<0.005, *** p<0.0005, **** p<0.0001 based on a two-way one-sample t-test or two-sided t-test.
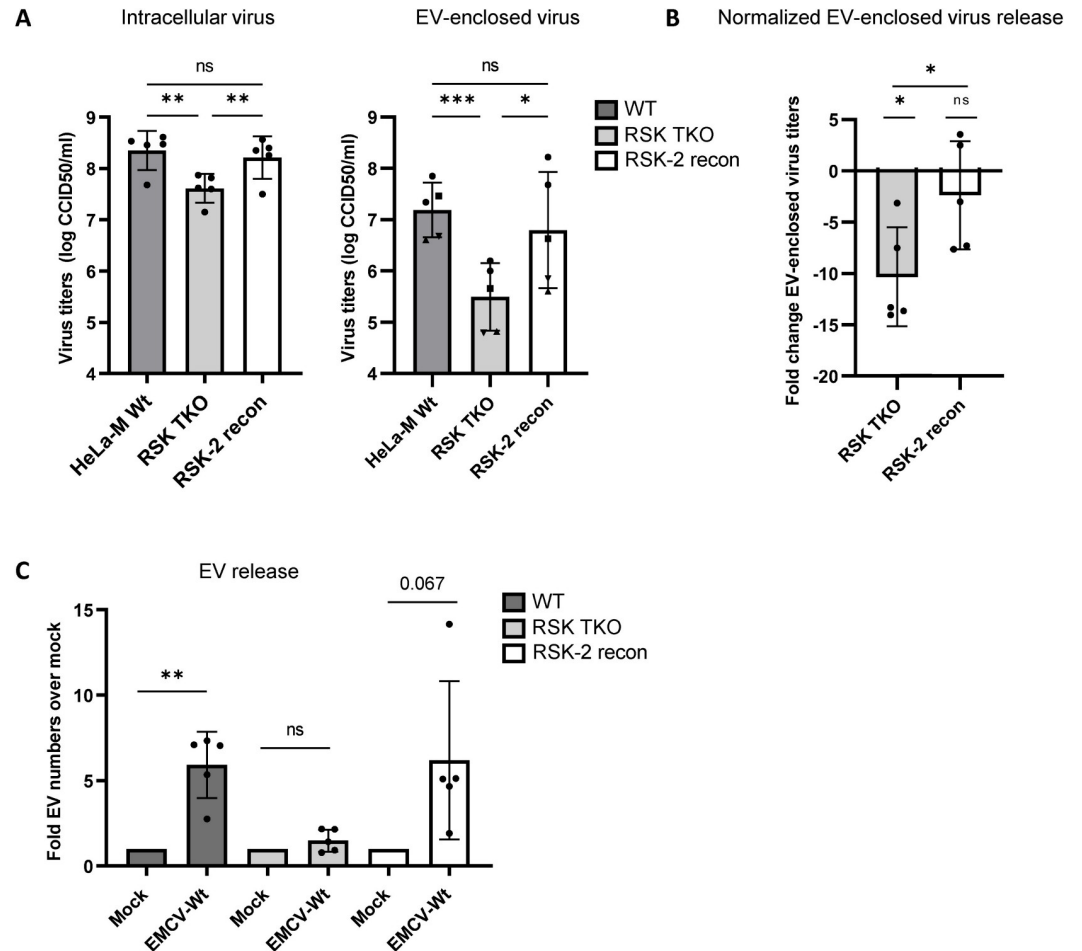
Fig 4. The EMCV Leader requires the host kinase RSK to promote EV release during infection. Hela-M WT cells, RSK-1/2/3 triple KO (TKO) cells, and TKO cells reconstituted with RSK-2 were mock infected or infected with EMCV-Wt. 7 hpi EVs were isolated from the supernatant of (mock) infected cells. (A) Intracellular virus titers and EV-enclosed virus titers were determined by end-point dilution assay. *** $p<0.0005$, * $p<0.05$ as determined by a RM one-way ANOVA with Geisser-Greenhouse correction. (B) Depicted is the fold change in EV-enclosed virus titers upon RSK TKO and RSK-2 reconstitution after correcting for the fold change in intracellular virus titers in the corresponding samples. * $p<0.05$ as determined by a two-tailed t-test or one-sample t-test. (C) EV numbers were quantified by high resolution flow cytometry. Depicted is the fold increase in EV numbers relative to the respective mock-infected controls. ** $p<0.005$ as determined by a two-tailed one-sample t-test. For (A-C) means ± SD of n = 5 independent experiments are shown.

EMCV-Wt that could explain the observed difference in efficiency by which these two sets of viruses modulate EV-enclosed virus release and induce secretory autophagy.

EMCV L was previously shown to promote the activation of the stress kinase P38 MAPK [34]. Notably, P38 has been described as an important regulator of EV release in response to various pro-inflammatory stimuli [45–50]. P38 activation has also been demonstrated in response to CVB3 infection, and was shown to promote CVB3 virus release [51,52]. This prompted us to investigate a potential link between P38 activation by the picornavirus security proteins and the induction of EV-enclosed virus release. In EMCV-Wt and EMCV-2A[Pro] infected cells we observed increased levels of phosphorylated (activated) P38, whereas P38 activation was not observed for EMCV-L[Zn/TMEV/SAFV] infected cells at 7 or 10 hpi (Fig 5A). To assess whether the observed activation of P38 in EMCV-Wt and EMCV-2A[Pro] infected cells contributed to enhanced induction of EV and EV-enclosed virus release, cells were treated
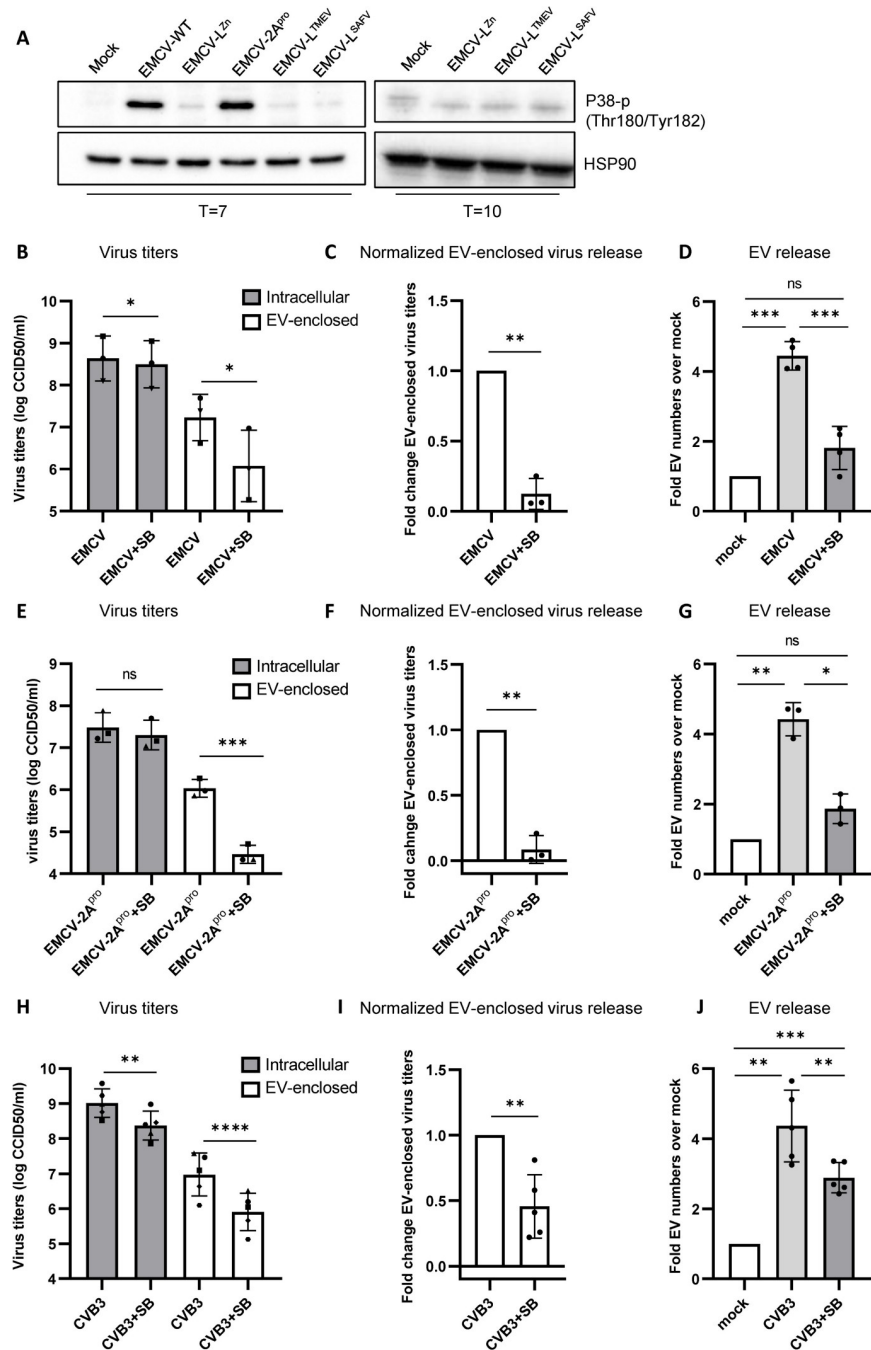
Fig 5. Activation of the stress kinase P38 MAPK in the presence of EMCV L and CVB3 2A^Pro, but not TMEV L and SAFV L, promotes EV and EV-enclosed virus release during infection. (A) Phosphorylated P38 MAPK (Thr 180/Tyr 182) was detected by western blot in whole cell lysates of mock-infected Hela cells or HeLa cells infected with the indicated (recombinant) viruses at 7 and 10 hpi. HSP90 was detected as loading control. Representative images of n = 3 independent experiments are shown. (B-G) EMCV-Wt (B-D) or EMCV-2A^Pro (E-G) infected cells were treated with 10 μM of the P38 inhibitor SB203580 (SB) 1 hpi. (B,E) Intracellular and EV-enclosed virus titers 7 hpi were determined using end-point dilution assay. (C,F) Quantification of the fold change in EV-enclosed virus titers upon treatment with the P38 inhibitor SB, after correction for differences in intracellular virus production in the corresponding samples. (D, G) EV numbers were quantified by high resolution flow cytometry. Depicted is the fold increase in EV numbers during infection relative to the respective mock-infected controls. (H-J) Experiments indicated above were repeated for CVB3-Wt infected cells treated with 50 μM SB starting 30 min pre-infection. * $p < 0.05$, ** $p < 0.005$, ***$p < 0.0005$, ****$p < 0.0001$ as determined by a paired two-tailed t-test or one-sample t-test. Bar graphs display mean ±SD of n = 3–5 independent samples.

with a low dose of P38 inhibitor SB203580 (SB). The inhibitor had a minimal effect on EMCV-Wt intracellular virus titers, but lead to a clear reduction in EV-enclosed virus release (Fig 5B and 5C). In addition, we observed that P38 inhibition largely abolished the induction of overall EV release in response to infection (Fig 5D). P38 inhibition also strongly inhibited the release of EVs and EV-enclosed viruses in response to infection with EMCV-2A^{pro}, whereas no reduction of intracellular virus titers was observed (Fig 5E–5F). In support of these data, we confirmed that inhibition of P38 in cells infected with wild type CVB3 also led to reduced release of EVs and EV-enclosed virus, albeit with a smaller effect size (Fig 5H–5J). Hence, our data highlights a differential capacity of picornavirus security proteins to promote the activation of the P38 stress pathway, and implicates this pathway as a positive regulator for the production of virus-carrying EVs during infection.

Collectively, these data provide new insights into the determinants of EV-enclosed virus release. We show that both the inhibition of the PKR antiviral stress pathway and the activation of the stress kinase P38 pathway regulate the production of EVs and EV-enclosed virions during EMCV infection. Picornavirus security proteins that modulate both pathways are most efficient in inducing the release of virus-carrying EV subsets.

Discussion

In this study we made use of a recombinant virus expression system to allow for the direct side-by-side comparison of the impact of different picornavirus security proteins on EV and EV-enclosed virus release. Using this approach, we show that functionally related non-structural proteins encoded by viruses belonging to different genera in the family *Picornaviridae* can promote the release of EV-enclosed virus. The Leader proteins of three different members of the genus *Cardiovirus* (i.e. EMCV, TMEV and SAFV) as well as the 2A^{pro} protein of CVB3, a member of the genus *Enterovirus*, all promoted virus packaging within EVs, albeit with different efficiencies. Of these proteins, EMCV L and CVB3 2A^{pro} induced a more rapid and prominent increase in EV-enclosed virus release, correlating with an increase in overall EV production and the induction of flotillin+, LC3+, FSC-high EV subsets. These findings highlight differences in the capacity of these viral proteins to induce EV-enclosed virus release, providing an opportunity to explore the cellular pathways involved in this process.

Using knock out cells we were able to show that suppression of MAVS-mediated IFN induction, a prominent antiviral pathway inhibited by picornaviral security proteins, does not contribute to the induction of EV release during EMCV infection. Previous studies implied an inhibitory effect of IFN-stimulated genes on EV release in the context of infection with the picornavirus EV-A71 [10]. However, the short time window of EMCV replication, in combination with the fact that a single cycle infection was studied, may explain why we did not observe an impact of IFN induction on EMCV-induced EV release.

In contrast to MAVS, deletion of PKR, the antiviral sensor responsible for the formation of stress granules, partially restored the inability of EMCV lacking expression of its security protein EMCV L to induce EV and EV-enclosed virus release. In line with this finding, we observed that the induction of virus-induced EV subsets by EMCV L required the host factor RSK, a host kinase that was recently implicated in the inhibition of PKR by cardioviruses [31,53]. Together, these data suggest that PKR signaling acts as a negative regulator of EV-enclosed virus during infection. Interestingly, knock down of PKR has previously also been described to potentiate EV release in response to the expression of prion proteins [54]. Yet, the mechanism by which PKR signaling affects EV release remains unknown. Whereas cardiovirus Leader proteins mediate partial inhibition of PKR activation itself, CVB3 2A^{pro} inhibits stress granule formation downstream of PKR through mechanisms that remain incompletely

understood [38]. However, it remains to be investigated whether stress granule formation is the sole pathway explaining the inhibitory effect of PKR signaling on EV release. Importantly, we observed that TMEV L and SAFV L had a significantly lower capacity to promote EV and EV-enclosed virus release than EMCV L, despite comparable efficiencies in inhibiting PKR signaling and stress granule formation. Combined, the data indicate that virus-induced EV release in our system requires inhibition of PKR activation and is potentiated by PKR KO. Yet, the (partial) inhibition of PKR mediated by viral proteins such as TMEV L and SAFV L is not sufficient to prompt the production of virus-carrying EV subsets seen in the presence of EMCV L/CVB3 2A^{pro}.

We show that CVB3 2A^{pro} and EMCV L, but not TMEV/SAFV L, share the ability to promote P38 activation during EMCV infection, and that this is required for induction of EV production and enhanced EV-enclosed virus release. P38 is a central hub for cellular stress pathways and can be activated by a wide variety of stimuli [55]. Transfection of cells with EMCV L was previously shown to be sufficient to induce P38 phosphorylation [34]. This was independent of upstream MAPKKK/MAPKK kinases [34], and may be caused by inhibition of protein phosphatases through EMCV L protein-binding domains. In line with our observation that the cardiovirus Leaders differ in their ability to activate P38, EMCV L was previously shown to employ both P38 and the ERK-RSK pathways to modulate host cell behavior, whereas TMEV L was found to rely predominantly on RSK [31,34,53]. P38 activation has also frequently been described during CVB3 infection [51,52], however the mechanism behind this activation remains elusive. Our data points to a (supporting) role for CVB3 2A^{pro} in this process. For both EMCV and CVB3 WT viruses we confirmed that inhibition of P38 led to a reduction of virus-induced EV release. While the main function previously attributed to the activation of P38 by EMCV L is supporting the induction of NCTD [34], CVB3 2A^{pro} is capable of inducing NCTD through direct cleavage of the nucleopore complex protein Nup98 [40]. Therefore, the observed importance of P38 for EV and EV-enclosed virus release in both EMCV-Wt, EMCV-2A^{pro}, and CVB3 infected cells is unlikely to be explained through interference in virus-induced NCTD. Our data indicate that increased release of EV-enclosed viruses is rapidly followed by a loss of cell integrity. The induction of EV-enclosed virus release may therefore be part of a strong cellular stress response, regulated by both P38 and PKR stress pathways, which precedes infection-induced cell death.

In line with our findings in virus-infected cells, P38 has been implicated as a regulator of EV induction in response to various other pro-inflammatory stimuli, including extracellular ATP (eATP), TNF-α, high glucose, and triggering of the platelet-activating factor receptor [45–50]. Release of EVs in response to many of these stimuli was shown to be mediated by acid sphingomyelinase (A-SMase), a lysosomal sphingomyelinase that upon secretion promotes plasma membrane fluidity and subsequent budding to form EVs [47,48,50]. For eATP stimulation, P38 activation was required to increase overall cellular A-SMase activity [50]. In addition, P38 may be involved in the delivery of A-SMase to the plasma membrane, as P38 activity was implicated in relocalization of lysosomes to the cell periphery [56]. Together, these data prompt further investigation into the role of A-SMase in the release of EVs during EMCV and CVB3 virus infection.

In previous work we showed that induction of secretory autophagy contributes to the packaging of virus in EVs during EMCV and CVB3 infection [22,25]. During EMCV infection, the induction of secretory autophagy coincides with a decrease in the efficiency of autolysosome formation [25]. Recruitment of P38 to autophagosomes has been shown to inhibit autophagosome-lysosome fusion via ATG5 phosphorylation [57]. Hence, the observed P38 activation promoted by EMCV L and CVB3 2A^{pro}, but not TMEV/SAFV L, potentially contributes to the observed induction of secretory autophagy. Currently, little is known about the regulation of

the secretory autophagy pathway. Known triggers for the release of proteins via secretory autophagy include ER stress and proinflammatory signaling, among which inflammasome activation [58–62]. We propose that by affecting cellular stress responses, viral proteins such as EMCV L and CVB3 2A^{Pro} contribute to a cell stress phenotype that may promote the activation of such proinflammatory signaling cascades.

An important observation of this study is that the modulation of cellular stress pathways by viral proteins can lead to the activation of specific EV formation pathways in response to infection, and the packaging of virus particles in defined EV subsets. This is important because the type of EV that encloses a virion may influence the functional properties of the particle. Within an EV, a virion is co-packaged with host-derived molecules, which may influence how EV-enclosed virions contribute to the infection. Motifs within the EV membrane, such as integrins and exposed PS lipids, can vary between EV subsets and have been described to affect the biodistribution of EVs *in vivo* as well as the preferential binding to and uptake of EVs in different cell types (reviewed in [63,64]). In addition, different EV subsets can contain different host-derived signaling molecules that are co-incorporated with the virions. These molecules may trigger proinflammatory responses that could limit infection, such as mitochondrial DNA or other DAMPS [65,66], but can also possess proviral functions. For example, enterovirus A71 infected cells were shown to release EVs containing miR-146a, which increased the infection efficiency of virus particles enclosed in the same EV isolates [10]. Our data provides initial evidence that different virus-carrying EVs may be released depending on the type of molecular virus-host interactions occurring inside a cell, prompting further investigations into the functional heterogeneity among EV-enclosed virus particles.

Overall, the findings of this study shed new light on host and virus-encoded regulators of EV-enclosed virus release. We show that multiple picornavirus security proteins share the capacity to promote EV-enclosed virus release during infection. Importantly, the host proteins PKR and P38 MAPK, identified here as modulators of EV release during infection, are known to be widely targeted by a broad range of viruses. In addition to the *picornaviridae*, SARS-CoV-2, influenza A virus, herpes simplex 1, hepatitis C virus, HIV, rotavirus, and many more viruses have been shown to activate P38 to promote infection [67,68]. Similarly, viral factors with the ability to prevent PKR antiviral signaling are widespread throughout the viral kingdom [69]. In addition to known effects of P38 and PKR on virus replication and/or assembly, our work points to an impact of these host kinases on EV-mediated spreading of viruses, which further emphasizes their potential as therapeutic targets.

Materials and methods

Cells and viruses

Human cervical carcinoma cells (HeLa R19) and baby hamster kidney cells (BHK21) were purchased from the American Type Culture Collection (Rockville, MD), and buffalo green monkey cells (BGM) from the European Cell Culture Collection (ECACC). The production of PKR and MAVS KO HeLa R19 cells by CRISPR-Cas9 gene editing has been described elsewhere [70,71]. HeLa M WT, RSK-1/2/3 triple KO, and RSK-2 reconstituted cells were a kind gift from dr. prof. T. Michiels (de Duve Institute, Université Catholique de Louvain, Belgium) and have been described in [53]. All cell lines were cultured in Dulbecco's Modified Eagle Medium (high glucose, GlutaMAX, ThermoFischer Scientific, Waltham, MA, USA), supplemented with 10% fetal calf serum (FCS; GE Healthcare Bio-Sciences, Chicago, IL), 100 U/mL penicillin and 100 μg/mL streptomycin (Gibco, Paisley, United Kingdom) and kept in a humidified incubator at 37°C and 5% CO_2.

EMCV-Wt and recombinant viruses were produced using the previously described M16.1 infectious cDNA clone of mengovirus containing a shortened poly-C tract [72]. In this clone, C19A, C22A point mutations were introduced to inactivate the EMCV Leader protein (EMCV-L^{Zn}) [27]. Recombinant EMCV viruses were generated as described previously [70]. In brief, the coding sequences for TMEV L, SAFV L, and CVB3 2A^{pro} were amplified from infectious cDNA clones of CVB3 Nancy, TMEV DA1, and SAFV3 NL2007 [73–75]. PCR primers were flanked by XhoI/NotI restriction sites and the genes inserted into the corresponding restriction sites of the pStrep2-VFETQG-C19A-C22A-M16.1 infectious clone. In this clone, genes of interest are fused to the polyprotein of EMCV-L^{Zn} separated by a strep2 tag and a 3C cleavage site to liberate the protein of interest from the EMCV polyprotein after production. For CVB3 2A^{pro} the strep2 tag was omitted. A C109A mutation was introduced in CVB3 2A^{pro} by site-directed mutagenesis to generate the catalytically inactive version of CVB3 2A (2A^{mut}) [38]. For EMCV virus stock production, *in vitro* transcribed run-off RNA transcripts were transfected into BHK-21 cells. For CVB3 WT virus stock production, run-off transcripts of the p53CB3/T7 infectious clone containing CVB3 strain Nancy were transfected in BGM cells [74]. Upon the observation of complete cytopathogenic effect (CPE), samples were subjected to three consecutive freeze-thaw cycles. Cell debris was removed by centrifugation for 30 min at 3000x*g* and virus purified by pelleting through a 30% sucrose cushion at 25,000 rpm for 15 hrs in a SW32 rotor (k-factor 321) (Beckman Coulter, Brea, CA).

Antibodies

The following antibodies were used for western blotting: mouse-α-CD9 (1:2000, clone HI9a; Biolegend, San Diego, CA), mouse-α-Flotillin-1 (1:1000, clone 18/Flotillin-1; BD Biosciences), mouse-α-LC3 (1:500, clone 5F10, Nanotools, Teningen, Germany), rabbit-α-LC3 (1:1000, polyclonal; MBL international, Woburn, MA), rabbit-α-phospho P38 MAPK (1:2000, polyclonal, Promega), mouse-α-HSP90 (1:1000, clone 68/HSP90, BD Biosciences), rabbit-α-phospho PKR (1:1000, clone E120; Abcam), mouse-α-actin (1:30,000, clone AC-15, Sigma-Aldrich), mouse-α-GAPDH (1:2000, clone mAbcam 9484; Abcam), HRP-coupled goat-α-mouse secondary antibody (1:10,000; Jackson ImmunoResearch Labaratories Inc., West Grove, PA), goat-α-rabbit secondary antibody (1:2500, P0448, DAKO, Denmark). For immunofluorescence staining cells were stained with rabbit-α-G3BP1 (1:150, polyclonal, Aviva, San Diego, CA), mouse-α-hnRNPK (1:100, clone D-6, Santa Cruz), goat-α-mouse or goat-α-rabbit Alexa488 and 647 (1:200, polyclonal, Invitrogen, MA), donkey-α-mouse Alexa488 and 647 (1:200, polyclonal, Thermo Fischer Scientific).

EV isolation

Cells were infected at a multiplicity of infection (MOI) of 10. After 1hr incubation, cells were washed three times with PBS +Ca+Mg and incubated with cell culture medium containing 10% EV-depleted FCS. To this generate EV-depleted FCS, FCS was prediluted 1:3 in DMEM, ultracentrifuged for 16–20 hrs at 28,000 rpm in an SW32 rotor (k-factor 256.8) and passed through a 0.22 μm filter. For inhibition of P38 during EMCV-Wt/EMCV-2A^{pro} infection, EV-depleted medium was supplemented with 10 μM SB203580 (Selleckchem, The Netherlands). For CVB3 samples, 50 μM SB203580 was added 30 min prior to infection and maintained in the medium all steps thereafter as described previously [52]. At the indicated time points post infection, cell culture supernatants were harvested and centrifuged 10 min at 200x*g* and 2x 10 min at 500x*g* to remove cells and cell debris. For recombinant virus infection experiments, samples were in addition treated with 100 μg/ml DNase I (Roche) for 45 min at 37˚C prior to EV isolation. EVs were isolated from clarified supernatants by UC pelleting for 65 min at

28,000 rpm in an SW40 rotor (k-factor 144.5) or by polyethylene glycol (PEG) precipitation o/n (10% PEG6000, 75mM NaCl, 5mM EDTA, 75mM Tris-HCl). EV pellets were resuspended in PBS or PBS +0.1% BSA (cleared from aggregates by ultracentrifugation for 16–20 hrs at 100,000xg). Next, EVs were mixed with iodixanol (Optiprep; Axis-Shield, Oslo, Norway) to a final concentration of 45% and overlaid with a linear gradient of 40%-5% iodixanol in PBS. Density gradients were centrifuged at 192,000xg for 16 hrs in a SW40 rotor. Gradient fractions of 1 mL were collected from the top and their densities assessed by refractometry. Individual gradient fractions were analyzed for their EV/virus content and the data of fractions within the density range of EVs (1.10–1.06 g/ml) was pooled for analysis unless otherwise indicated.

Virus titration

Virus titers in EVs were determined by performing end-point dilution assay. BHK-21 cells or HeLa-R19 cells were infected with 3 to 5-fold serial dilutions of prediluted density gradient fractions, and virus titers expressed in Median Cell Culture Infectious Dose (CCID50) values were calculated 3 days after infection using the Spearman-Karber calculation method for EMCV and CVB3 respectively. For intracellular virus titration, adherent cells and cells pelleted from the cell culture supernatant were combined and freeze-thawed three times. Cell debris was removed by centrifugation for 10 min at 500xg prior to virus titration.

High resolution flow cytometry

For single particle characterization of EV release, EVs were fluorescently labeled with 30 μM CFSE (Invitrogen, Carlsbad, CA) for 1 hr at RT prior to purification by density gradient centrifugation. Individual gradient fractions were mixed vigorously with 2% PFA and fixed for 30 min at RT. Samples were diluted 1:20 in PBS immediately prior to high-resolution flow cytometric analysis on a BD Influx flow cytometer with optimized configuration, as previously reported [43,44]. In short, thresholding was applied on fluorescence generated by CFSE-labeled EVs passing the 488 nm laser. Fluorescent 200 nm polystyrene beads (FluoSpheres, Invitrogen) were used to calibrate the fluorescence, forward (FSC) and side (SSC) scattered light settings. Samples were measured at low pressure (sheath fluid: 5 PSI, sample: 4.2 PSI) using a 140 μm nozzle with event rates below 10,000 per second. Measurements were acquired in a fixed time window of 30 seconds to allow direct comparison of EV concentrations in parallel samples. For Fig 5J, samples were measured on the Cytek Aurora spectral flow cytometer instead, using optimized settings for the detection of small particles. A similar fluorescent thresholding approach was applied, and for each sample a fixed volume was measured to allow for quantitative comparison of EV release. Data analysis was performed using FlowJo v10.07 software (FlowJo LLC, Ashland, OR) or FCS express v3 (De Novo software, Los Angeles, CA).

Western blot

Trichloroacetic acid (TCA) precipitation was performed on pooled gradient fractions within the 1.10–1.06 g/ml density range to enable protein analysis of density gradient purified EVs. In brief, samples were supplemented with 125 μg/ml sodium deoxycholate and 10% ice-cold TCA and pelleted for 15 min at 15,000xg. Pellets were washed twice with ice-cold aceton and resuspended in Laemmli sample buffer (LSB: 62.5 mM Tris-HCl pH 6.8, 2% SDS, 10% glycerol) with or without 20 mM 2-mercaptoethanol. For analysis of cells and UC pellets, samples were lysed in RIPA buffer (40 mM Tris-HCl pH 8, 0.5% sodium deoxycholate, 1% Triton X-100, 150 mM sodium chloride, 0.1% sodium dodecyl sulfate) supplemented with protease and phosphatase inhibitor cocktails (Roche) prior to mixing with LSB. Cell lysates were cleared by centrifugation at 15,000xg for 15 min and protein concentration was determined using a

Pierce BCA assay kit (Thermo Fischer Scientific, Waltham, MA) according to the manufacturer's protocol. For purified EVs or UC pellets, equal number of producing cells were used to normalize input. LC3-I and LC3-II positive controls were purchased from Nanotools (Teningen, Germany). Proteins were denatured by incubating 4 min at 98˚C, separated on sodium dodecyl sulfate-polyacrylamide gels by electrophoresis (SDS-PAGE), and transferred to Immobilon PVDF membranes (Merck Millipore Ltd., Cork, Ireland) by wet transfer. Membranes were blocked with 0.25% (v/v) fish skin gelatin (FSG; Sigma-Aldrich) or 5% BSA in PBS + 0.1% tween (PBS-T) for 1 hr at RT, followed by incubation o/n with primary antibodies. Membranes were washed 5x in 0.25% (v/v) FSG or 0.5–1% BSA in PBS-T followed by incubation for 45 min at RT with secondary antibodies. After 3x wash in PBS-T and $\geq$2x wash in PBS, membranes were developed using ECL solution (SuperSignal West Dura Extended Duration Substrate, Thermo Fischer Scientific) for detection on a Bio-Rad ChemiDoc imager. Images were analyzed by Image Lab software (Bio-Rad). For the detection of phosphoproteins, PBS was replaced with Tris-buffered saline in all buffers.

Cell permeability assay

To assess the proportion of permeable cells, cells were harvested by trypsinization and pooled with any detached cells recovered from the supernatant following centrifugation at 200xg for 10 min. Cells were washed twice in ice cold PBS followed by staining on ice for 30 min using 1:1000 diluted Fixable Viability Dye eFluor 506 (eBioscience, San Diego, CA) according to manufacturer's instructions. Unbound dye was removed by washing with PBS and the cells were fixed in 1–2% PFA. Cells were analyzed using a CytoFLEX LX (Beckman Coulter). Data analysis was performed using FlowJo. Heat shocked cells were taken along in all experiments as positive control. To this end, cells were incubated for 3 min at 65˚C followed by immediate placement on ice for 1 min.

Immunofluorescence staining

Cells were fixed with 4% PFA 6–7 hpi and permeabilized by incubation with 0.1% Triton X-100 for 10 min. Samples were washed and incubated in block buffer (PBS + 2% BSA + 50mM NH_4Cl) for 30 min prior to staining for 45 min with primary antibodies diluted in block buffer. After three washes with block buffer, antibody labelling was repeated with secondary antibodies plus 300nM DAPI. Finally, coverslips were washed in block buffer followed by MiliQ before being mounted in FluorSafe (Calbiochem, San Diego, CA) or ProLong Diamond Antifade Mountant (Thermo Fischer Scientific). Samples were imaged using a 60x or 100x CFI PLAN APO oil objective on a Nikon A1R confocal microscope with hardware settings to image the relevant channels sequentially using recommended emission spectral filter settings. Images were processed using ImageJ software.

Quantitative reverse transcription PCR (RT-qPCR)

Total RNA from cells was extracted using NucleoSpin RNA kit (MACHEREY-NAGEL GmbH & Co. KG). Reverse transcription was performed with the RevertAid first-strand cDNA synthesis kit (Thermo Scientific, CA, USA). The levels of IFN-β RNA were detected by RT-qPCR using Fast SYBR Green Master Mix (Thermo Fisher Scientific, USA) and LightCycler 480 real-time PCR detection system (Roche). The thermal cycling conditions were composed of an initial denaturation step at 95˚C for 5 min, 45 cycles at 95˚C for 10s, 60˚C for 5s and 72˚C for 30s. The experiments were carried out in duplicate for each data point. The primer sequences used for quantification were as follows: IFN-β: Fw 5' ATGACCAACAAGTGTCTCCTCC 3',

Rev: 5' GCTCATGGAAAGAGCTGTAGTG 3'. β-Actin: Fw 5' CCTTCCTGGGCATG-GAGTCCTG 3', Rev: 5' GGAGCAATGATCTTGATCTTC 3'.

Statistical analysis

Data display and analysis was performed using GraphPad Prism version 9 (GraphPad Software, CA).

Supporting information

S1 Fig. TMEV L, SAFV L, and CVB3 2A^{pro} can suppress stress granule formation, induce NCTD, and prevent IFN-β induction during infection with EMCV-L^{Zn}. Cells were infected with EMCV-Wt, EMCV-L^{Zn}, or recombinant viruses in which the coding sequences of TMEV L (L^{TMEV}), SAFV L (L^{SAFV}), or CVB3 2A (2A^{pro}) were fused to the polyprotein of EMCV-L^{Zn}. (A) Detection of phosphorylated PKR in whole cell lysates of infected cells compared to an uninfected control 7 hpi. (B) The formation of stress granules was monitored by staining for the stress granule marker G3BP1 (red) and DAPI (blue) in (mock) infected cells 6–6.5 hpi. For mock and EMCV-L^{SAFV} expressing samples, brightness was increased 20% to allow visualization of the diffuse signal. (C) The induction of NCTD was monitored by analyzing changes in the cellular distribution of the nuclear protein hnRNPK (hot cyan) compared to DAPI (red). Representative images of n = 3 independent experiments are shown. (D) IFN-β mRNA levels were determined by RT-qPCR 6–6.5 hpi. Bar graphs display the mean IFN-β expression levels ± SD relative to those detected in EMCV-L^{Zn} infected samples (set to 100%) of n = 3 independent experiments. $^{**}p<0.005$, $^{***}p<0.0005$ using a two-tailed one sample t-test. (TIF)

S2 Fig. Induction of extracellular virus release during infection with EMCV-Wt and EMCV-2A^{pro}. (A-B) Fold increase in extracellular virus titers observed during infection with the viruses EMCV-Wt and EMCV-2A^{pro} compared to EMCV-L^{Zn}. (A) Line graphs depicting results without normalization. (B) Line graph depicting results after normalization for differences in intracellular virus production. Plotted are means ±SD of n = 3–4 independent experiments. (TIF)

S3 Fig. Cell permeability upon infection with EMCV recombinant viruses. (A) The percentage of cells maintaining plasma membrane integrity over the course of infection was measured by staining cells with a cell impermeable dye followed by flow cytometric analysis. Line graphs depict mean ± SD of n = 2–3 independent experiments. (TIFF)

S4 Fig. The impact of reconstitution of EMCV-L^{Zn} with proteolytically active or inactive CVB3 2A^{pro} on intracellular virus titers and EV release. Cells were infected with EMCV-L^{Zn}, EMCV-L^{Zn} reconstituted with CVB3 2A^{pro} (EMCV-2A^{pro}) or with a mutated version of CVB3 2A that lacks proteolytic activity (EMCV-2A^{mut}). (A) Intracellular virus titers were compared 7 hpi using end-point dilution assay. (B) EV numbers were quantified by high resolution flow cytometry. Depicted are the EV numbers relative to the respective mock-infected samples. ns, $p>0.05$, $p^{**}<0.005$, $^{***}p<0.0001$ as determined by one-way ANOVA with Tukey's multiple comparisons test. Bar graphs display mean ±SD of n = 3 independent experiments. (TIF)

S5 Fig. Analysis of LC3 in gradient purified EVs upon EMCV recombinant virus infection. Depicted are the expanded western blots shown in Fig 2D including the positive controls for

LC3I and LC3II, measured using short (top) and long (bottom) exposure times. Depicted are representative images of n = 2 independent experiments.
(TIF)

S6 Fig. Knock out of the antiviral sensor PKR, but not MAVS, rescues FSC^{high} EV release during infection with EMCV-L^{Zn}. PKR KO (A) and MAVS KO (B) cells were infected with EMCV-Wt or EMCV-L^{Zn} at MOI 10. 7 hpi EVs were isolated by density gradient centrifugation and light scattering patterns induced by EVs were assessed by high resolution flow cytometry. Bar graphs display the percentage of EVs that display a high degree of forward-scattered light (FSC^{high}), based on the gating strategy depicted in Fig 3D. Depicted are means ±SD of n = 3/4 independent samples. * $p < 0.05$, ** $p < 0.005$ determined by one-way ANOVA with Tukey's multiple comparisons test.
(TIF)

S1 Data. Source data file containing individual numerical data points for each of the graphs in this manuscript.
(XLSX)

Acknowledgments

Author Contributions

Conceptualization: Kyra A. Y. Defourny, Frank J. M. van Kuppeveld, Esther N. M. Nolte-´t Hoen.

Formal analysis: Kyra A. Y. Defourny, Xinyi Pei.

Funding acquisition: Esther N. M. Nolte-´t Hoen.

Investigation: Kyra A. Y. Defourny, Xinyi Pei.

Methodology: Kyra A. Y. Defourny, Frank J. M. van Kuppeveld.

Supervision: Frank J. M. van Kuppeveld, Esther N. M. Nolte-´t Hoen.

Writing – original draft: Kyra A. Y. Defourny.

Writing – review & editing: Kyra A. Y. Defourny, Esther N. M. Nolte-´t Hoen.

References

1. Yáñez-Mó M, Siljander PRM, Andreu Z, Bedina Zavec A, Borràs FE, Buzas EI, et al. Biological properties of extracellular vesicles and their physiological functions. J Extracell Vesicles. 2015 Jan 14; 4 (1):27066. https://doi.org/10.3402/jev.v4.27066 PMID: 25979354

2. Chen YH, Du W, Hagemeijer MC, Takvorian PM, Pau C, Cali A, et al. Phosphatidylserine vesicles enable efficient en bloc transmission of enteroviruses. Cell. 2015 Feb 12; 160(4):619–30. https://doi.org/10.1016/j.cell.2015.01.032 PMID: 25679758

3. Gu J, Wu J, Fang D, Qiu Y, Zou X, Jia X, et al. Exosomes cloak the virion to transmit Enterovirus 71 non-lytically. Virulence. 2020 Jan 1; 11(1):32–8. https://doi.org/10.1080/21505594.2019.1705022 PMID: 31885311

4. van der Grein SG, Defourny KAY, Rabouw HH, Galiveti CR, Langereis MA, Wauben MHM, et al. Picornavirus infection induces temporal release of multiple extracellular vesicle subsets that differ in

molecular composition and infectious potential. PLoS Pathog. 2019 Feb 1; 15(2). https://doi.org/10.1371/journal.ppat.1007594 PMID: 30779790

5. Netanyah E, Calafatti M, Arvastsson J, Cabrera-Rode E, Cilio CM, Sarmiento L. Extracellular Vesicles Released by Enterovirus-Infected EndoC-βH1 Cells Mediate Non-Lytic Viral Spread. Microorganisms. 2020 Nov 1; 8(11):1–13. https://doi.org/10.3390/MICROORGANISMS8111753 PMID: 33171580

6. Santiana M, Ghosh S, Ho BA, Rajasekaran V, Du WL, Mutsafi Y, et al. Vesicle-Cloaked Virus Clusters Are Optimal Units for Inter-organismal Viral Transmission. Cell Host Microbe. 2018 Aug 8; 24(2):208–220.e8. https://doi.org/10.1016/j.chom.2018.07.006 PMID: 30092198

7. Yin X, Ambardekar C, Lu Y, Feng Z. Distinct Entry Mechanisms for Nonenveloped and Quasi-Enveloped Hepatitis E Viruses. J Virol. 2016 Apr 15; 90(8):4232–42. https://doi.org/10.1128/JVI.02804-15 PMID: 26865708

8. Labadie T, Roy P. A non-enveloped arbovirus released in lysosome-derived extracellular vesicles induces super-infection exclusion. PLoS Pathog. 2020 Oct 19; 16(10). https://doi.org/10.1371/journal.ppat.1009015 PMID: 33075107

9. Kerviel A, Zhang M, Altan-Bonnet N. A New Infectious Unit: Extracellular Vesicles Carrying Virus Populations. Annu Rev Cell Dev Biol. 2021; 37:171–97. https://doi.org/10.1146/annurev-cellbio-040621-032416 PMID: 34270326

10. Fu Y, Zhang L, Zhang F, Tang T, Zhou Q, Feng C, et al. Exosome-mediated miR-146a transfer suppresses type I interferon response and facilitates EV71 infection. PLoS Pathog. 2017 Sep 14; 13(9): e1006611. https://doi.org/10.1371/journal.ppat.1006611 PMID: 28910400

11. O'Hara BA, Morris-Love J, Gee G v, Haley SA, Atwood WJ. JC Virus infected choroid plexus epithelial cells produce extracellular vesicles that infect glial cells independently of the virus attachment receptor. PLoS Pathog. 2020; 16(3). https://doi.org/10.1371/journal.ppat.1008371 PMID: 32130281

12. Morris-Love J, Gee G v., O'Hara BA, Assetta B, Atkinson AL, Dugan AS, et al. JC polyomavirus uses extracellular vesicles to infect target cells. mBio. 2019 Mar; 10(2). https://doi.org/10.1128/mBio.00379-19 PMID: 30967463

13. Mao L, Wu J, Shen L, Yang J, Chen J, Xu H. Enterovirus 71 transmission by exosomes establishes a productive infection in human neuroblastoma cells. Virus Genes. 2016 Apr 2; 52(2):189–94. https://doi.org/10.1007/s11262-016-1292-3 PMID: 26837894

14. Feng Z, Hensley L, McKnight KL, Hu F, Madden V, Ping L, et al. A pathogenic picornavirus acquires an envelope by hijacking cellular membranes. Nature. 2013 Apr 18; 496(7445):367–71. https://doi.org/10.1038/nature12029 PMID: 23542590

15. Nagashima S, Takahashi M, Kobayashi T, Tanggis T, Nishizawa T, Nishiyama T, et al. Characterization of the Quasi-Enveloped Hepatitis E Virus Particles Released by the Cellular Exosomal Pathway. J Virol. 2017 Nov 15; 91(22):e00822–17. https://doi.org/10.1128/JVI.00822-17 PMID: 28878075

16. György B, Fitzpatrick Z, Crommentuijn MHW, Mu D, Maguire CA. Naturally enveloped AAV vectors for shielding neutralizing antibodies and robust gene delivery in vivo. Biomaterials. 2014 Aug; 35 (26):7598–609. https://doi.org/10.1016/j.biomaterials.2014.05.032 PMID: 24917028

17. Chapuy-Regaud S, Dubois M, Plisson-Chastang C, Bonnefois T, Lhomme S, Bertrand-Michel J, et al. Characterization of the lipid envelope of exosome encapsulated HEV particles protected from the immune response. Biochimie. 2017 Oct; 141:70–9. https://doi.org/10.1016/j.biochi.2017.05.003 PMID: 28483690

18. Iša P, Pérez-Delgado A, Quevedo IR, López S, Arias CF. Rotaviruses Associate with Distinct Types of Extracellular Vesicles. Viruses. 2020 Jul 1; 12(7). https://doi.org/10.3390/v12070763 PMID: 32708544

19. Quevedo IR, López S, Arias CF, Iša P. The association of human astrovirus with extracellular vesicles facilitates cell 1 infection and protects the virus from neutralizing antibodies. https://doi.org/10.1101/2021.05.17.444590

20. Jiang W, Ma P, Deng L, Liu Z, Wang X, Liu X, et al. Hepatitis A virus structural protein pX interacts with ALIX and promotes the secretion of virions and foreign proteins through exosome-like vesicles. J Extracell Vesicles. 2020 Jan 1; 9(1). https://doi.org/10.1080/20013078.2020.1716513 PMID: 32082513

21. Huang HI, Lin JY, Chiang HC, Huang PN, Lin QD, Shih SR. Exosomes Facilitate Transmission of Enterovirus A71 From Human Intestinal Epithelial Cells. J Infect Dis. 2020 Aug 1; 222(3):456. https://doi.org/10.1093/infdis/jiaa174 PMID: 32271384

22. Giansanti P, Strating JRPM, Defourny KAY, Cesonyte I, Bottino AMS, Post H, et al. Dynamic remodelling of the human host cell proteome and phosphoproteome upon enterovirus infection. Nat Commun. 2020 Dec 1; 11(1). https://doi.org/10.1038/s41467-020-18168-3 PMID: 32859902

23. Sin J, McIntyre L, Stotland A, Feuer R, Gottlieb RA. Coxsackievirus B Escapes the Infected Cell in Ejected Mitophagosomes. J Virol. 2017 Dec 15; 91(24):e01347–17. https://doi.org/10.1128/JVI.01347-17 PMID: 28978702

24. Bird SW, Maynard ND, Covert MW, Kirkegaard K. Nonlytic viral spread enhanced by autophagy components. Proc Natl Acad Sci U S A. 2014 Sep 9; 111(36):13081–6. https://doi.org/10.1073/pnas.1401437111 PMID: 25157142

25. van der Grein SG, Defourny KAY, Rabouw HH, Goerdayal SS, van Herwijnen MJC, Wubbolts RW, et al. The encephalomyocarditis virus Leader promotes the release of virions inside extracellular vesicles via the induction of secretory autophagy. Nat Commun. 2022 Dec 24; 13(1):3625. https://doi.org/10.1038/s41467-022-31181-y PMID: 35750662

26. Ponpuak M, Mandell MA, Kimura T, Chauhan S, Cleyrat C, Deretic V. Secretory autophagy. Curr Opin Cell Biol. 2015 Aug; 35:106–16. https://doi.org/10.1016/j.ceb.2015.04.016 PMID: 25988755

27. Hato S v., Ricour C, Schulte BM, Lanke KHW, de Bruijni M, Zoll J, et al. The mengovirus leader protein blocks interferon-α/β gene transcription and inhibits activation of interferon regulatory factor 3. Cell Microbiol. 2007 Dec; 9(12):2921–30. https://doi.org/10.1111/j.1462-5822.2007.01006.x PMID: 17991048

28. Freundt EC, Drappier M, Michiels T. Innate immune detection of cardioviruses and viral disruption of interferon signaling. Front Microbiol. 2018 Oct; 12(9):2448. https://doi.org/10.3389/fmicb.2018.02448 PMID: 30369921

29. Borghese F, Michiels T. The leader protein of cardioviruses inhibits stress granule assembly. J Virol. 2011 Sep 15; 85(18):9614–22. https://doi.org/10.1128/JVI.00480-11 PMID: 21752908

30. Langereis MA, Feng Q, van Kuppeveld FJ. MDA5 Localizes to Stress Granules, but This Localization Is Not Required for the Induction of Type I Interferon. J Virol. 2013 Jun 1; 87(11):6314–25. https://doi.org/10.1128/JVI.03213-12 PMID: 23536668

31. Sorgeloos F, Peeters M, Hayashi Y, Borghese F, Capelli N, Drappier M, et al. A case of convergent evolution: Several viral and bacterial pathogens hijack RSK kinases through a common linear motif. Proc Natl Acad Sci U S A. 2022 Feb 1; 119(5):e2114647119. https://doi.org/10.1073/pnas.2114647119 PMID: 35091472

32. Borghese F, Sorgeloos F, Cesaro T, Michiels T. The Leader Protein of Theiler's Virus Prevents the Activation of PKR. J Virol. 2019 Oct; 93(19). https://doi.org/10.1128/JVI.01010-19 PMID: 31292248

33. Ciomperlik JJ, Basta HA, Palmenberg AC. Three cardiovirus Leader proteins equivalently inhibit four different nucleocytoplasmic trafficking pathways. Virology. 2015 Oct; 484:194–202. https://doi.org/10.1016/j.virol.2015.06.004 PMID: 26115166

34. Porter FW, Brown B, Palmenberg AC. Nucleoporin phosphorylation triggered by the encephalomyocarditis virus leader protein is mediated by mitogen-activated protein kinases. J Virol. 2010 Dec 15; 84 (24):12538–48. https://doi.org/10.1128/JVI.01484-09 PMID: 20881039

35. Agol VI, Gmyl AP. Viral security proteins: Counteracting host defences. Nat Rev Microbiol; 2010 Dec; 8 (12):867–78. https://doi.org/10.1038/nrmicro2452 PMID: 21060318

36. Petty R v., Basta HA, Bacot-Davis VR, Brown BA, Palmenberg AC. Binding Interactions between the Encephalomyocarditis Virus Leader and Protein 2A. J Virol. 2014 Nov 15; 88(22):13503. https://doi.org/10.1128/JVI.02148-14 PMID: 25210192

37. Paul S, Michiels T. Cardiovirus leader proteins are functionally interchangeable and have evolved to adapt to virus replication fitness. J Gen Virol. 2006 May; 87(Pt 5):1237–46. https://doi.org/10.1099/vir.0.81642-0 PMID: 16603526

38. Visser LJ, Langereis MA, Rabouw HH, Wahedi M, Muntjewerff EM, Groot RJ de, et al. Essential Role of Enterovirus 2A Protease in Counteracting Stress Granule Formation and the Induction of Type I Interferon. J Virol. 2019 May 15; 93(10):222–41. https://doi.org/10.1128/JVI.00222-19 PMID: 30867299

39. Lidsky P v., Hato S, Bardina M v., Aminev AG, Palmenberg AC, Sheval E v., et al. Nucleocytoplasmic Traffic Disorder Induced by Cardioviruses. J Virol. 2006 Mar 15; 80(6):2705. https://doi.org/10.1128/JVI.80.6.2705-2717.2006 PMID: 16501080

40. Serganov AA, Udi Y, Stein ME, Patel V, Fridy PC, Rice CM, et al. Proteomic elucidation of the targets and primary functions of the picornavirus 2A protease. Journal of Biological Chemistry. 2022 Jun; 298 (6):101882. https://doi.org/10.1016/j.jbc.2022.101882 PMID: 35367208

41. Nchoutmboube JA, Viktorova EG, Scott AJ, Ford LA, Pei Z, Watkins PA, et al. Increased long chain acyl-Coa synthetase activity and fatty acid import is linked to membrane synthesis for development of picornavirus replication organelles. PLoS Pathog. 2013 Jun; 9(6). https://doi.org/10.1371/journal.ppat.1003401 PMID: 23762027

42. Diep J, Ooi YS, Wilkinson AW, Peters CE, Foy E, Johnson JR, et al. Enterovirus Pathogenesis Requires the Host Methyltransferase SETD3. Nat Microbiol. 2019 Dec; 4(12):2523. https://doi.org/10.1038/s41564-019-0551-1 PMID: 31527793

43. van der Vlist EJ, Nolte-'t Hoen ENM, Stoorvogel W, Arkesteijn GJA, Wauben MHM. Fluorescent labeling of nano-sized vesicles released by cells and subsequent quantitative and qualitative analysis by

high-resolution flow cytometry. Nat Protoc. 2012 Jun 14; 7(7):1311–26. https://doi.org/10.1038/nprot.2012.065 PMID: 22722367

44. Nolte-'t Hoen ENM, van der Vlist EJ, Aalberts M, Mertens HCH, Bosch BJ, Bartelink W, et al. Quantitative and qualitative flow cytometric analysis of nanosized cell-derived membrane vesicles. Nanomedicine. 2012 Jul; 8(5):712–20. https://doi.org/10.1016/j.nano.2011.09.006 PMID: 22024193

45. Ryu JH, Kim SJ. Clopidogrel effectively suppresses endothelial microparticle generation induced by indoxyl sulfate via inhibition of the p38 mitogen-activated protein kinase pathway. Blood Purif. 2011 Oct; 32(3):186–94. https://doi.org/10.1159/000326297 PMID: 21811066

46. Curtis AM, Wilkinson PF, Gui M, Gales TL, Hu E, Edelberg JM. p38 mitogen-activated protein kinase targets the production of proinflammatory endothelial microparticles. Journal of Thrombosis and Haemostasis. 2009 Apr 1; 7(4):701–9. https://doi.org/10.1111/j.1538-7836.2009.03304.x PMID: 19192109

47. Li M, Zhang X, Yu J, Wu X, Sun L. Monocyte-Derived Procoagulant Microvesicles Induced by High Glucose Can Be Attenuated by the Antioxidant N-Acetyl-L-Cysteine, Partly Through the P38/MAPK Pathway. Metab Syndr Relat Disord. 2017 Dec 1; 15(10):521–6. https://doi.org/10.1089/met.2017.0089 PMID: 29125808

48. Thyagarajan A, Kadam SM, Liu L, Kelly LE, Rapp CM, Chen Y, et al. Gemcitabine Induces Microvesicle Particle Release in a Platelet-Activating Factor-Receptor-Dependent Manner via Modulation of the MAPK Pathway in Pancreatic Cancer Cells. International Journal of Molecular Sciences 2019, Vol 20, Page 32. 2018 Dec 21; 20(1):32. https://doi.org/10.3390/IJMS20010032 PMID: 30577630

49. Chen Z, Schubert P, Bakkour S, Culibrk B, Busch MP, Devine D v. p38 mitogen-activated protein kinase regulates mitochondrial function and microvesicle release in riboflavin- and ultraviolet light–treated apheresis platelet concentrates. Transfusion (Paris). 2017 May 1; 57(5):1199–207. https://doi.org/10.1111/TRF.14035 PMID: 28236306

50. Bianco F, Perrotta C, Novellino L, Francolini M, Riganti L, Menna E, et al. Acid sphingomyelinase activity triggers microparticle release from glial cells. EMBO J. 2009 Apr 22; 28(8):1043–54. https://doi.org/10.1038/emboj.2009.45 PMID: 19300439

51. Jensen KJ, Garmaroudi FS, Zhang J, Lin J, Boroomand S, Zhang M, et al. An ERK–p38 subnetwork coordinates host cell apoptosis and necrosis during coxsackievirus B3 infection. Cell Host Microbe. 2013 Jan 16; 13(1):67. https://doi.org/10.1016/j.chom.2012.11.009 PMID: 23332156

52. Si X, Luo H, Morgan A, Zhang J, Wong J, Yuan J, et al. Stress-Activated Protein Kinases Are Involved in Coxsackievirus B3 Viral Progeny Release. J Virol. 2005 Nov 15; 79(22):13875. https://doi.org/10.1128/JVI.79.22.13875–13881.2005

53. Lizcano-Perret B, Lardinois C, Wavreil F, Hauchamps P, Herinckx G, Sorgeloos F, et al. Cardiovirus leader proteins retarget RSK kinases toward alternative substrates to perturb nucleocytoplasmic traffic. PLoS Pathog. 2022; 18(12):e1011042. https://doi.org/10.1371/journal.ppat.1011042 PMID: 36508477

54. Pataer A, Ozpolat B, Shao RP, Cashman NR, Plotkin SS, Samuel CE, et al. Therapeutic targeting of the PI4K2A/PKR lysosome network is critical for misfolded protein clearance and survival in cancer cells. Oncogene. 2020 Jan 23; 39(4):801. https://doi.org/10.1038/s41388-019-1010-4 PMID: 31554935

55. Canovas B, Nebreda AR. Diversity and versatility of p38 kinase signalling in health and disease. Nat Rev Mol Cell Biol. 2021 Jan 27; 22(5):346–66. https://doi.org/10.1038/s41580-020-00322-w PMID: 33504982

56. Willett R, Martina JA, Zewe JP, Wills R, Hammond GRV, Puertollano R. TFEB regulates lysosomal positioning by modulating TMEM55B expression and JIP4 recruitment to lysosomes. Nature Communications 2017 Nov 17; 8(1):1–17. https://doi.org/10.1038/s41467-017-01871-z PMID: 29146937

57. Keil E, Höcker R, Schuster M, Essmann F, Ueffing N, Hoffman B, et al. Phosphorylation of Atg5 by the Gadd45β–MEKK4-p38 pathway inhibits autophagy. Cell Death & Differentiation 2013 Feb; 20(2):321–32. https://doi.org/10.1038/cdd.2012.129 PMID: 23059785

58. Noh SH, Gee HY, Kim Y, Piao H, Kim J, Kang CM, et al. Specific autophagy and ESCRT components participate in the unconventional secretion of CFTR. Autophagy. 2018 Oct 3; 14(10):1761–78. https://doi.org/10.1080/15548627.2018.1489479 PMID: 29969945

59. Bel S, Pendse M, Wang Y, Li Y, Ruhn KA, Hassell B, et al. Paneth cells secrete lysozyme via secretory autophagy during bacterial infection of the intestine. Science. 2017 Sep 8; 357(6355):1047–52. https://doi.org/10.1126/science.aal4677 PMID: 28751470

60. New J, Thomas SM. Autophagy-dependent secretion: mechanism, factors secreted, and disease implications. https://doi.org/101080/1554862720191596479. 2019; 15(10):1682–93. PMID: 30894055

61. Wang Z, Zhou H, Zheng H, Zhou X, Shen G, Teng X, et al. Autophagy-based unconventional secretion of HMGB1 by keratinocytes plays a pivotal role in psoriatic skin inflammation. Autophagy. 2021; 17(2):529. https://doi.org/10.1080/15548627.2020.1725381 PMID: 32019420

62. Dupont N, Jiang S, Pilli M, Ornatowski W, Bhattacharya D, Deretic V. Autophagy-based unconventional secretory pathway for extracellular delivery of IL-1β. EMBO J. 2011 Nov 8; 30(23):4701–11. https://doi.org/10.1038/emboj.2011.398 PMID: 22068051

63. Kooijmans SAA, de Jong OG, Schiffelers RM. Exploring interactions between extracellular vesicles and cells for innovative drug delivery system design. Adv Drug Deliv Rev 2021 Jun; 173:252–78. https://doi.org/10.1016/j.addr.2021.03.017 PMID: 33798644

64. Kwok ZH, Wang C, Jin Y. Extracellular Vesicle Transportation and Uptake by Recipient Cells: A Critical Process to Regulate Human Diseases. Processes (Basel). 2021 Feb 1; 9(2):1–16. https://doi.org/10.3390/PR9020273 PMID: 34336602

65. Torralba D, Baixauli F, Villarroya-Beltri C, Fernández-Delgado I, Latorre-Pellicer A, Acín-Pérez R, et al. Priming of dendritic cells by DNA-containing extracellular vesicles from activated T cells through antigen-driven contacts. Nat Commun. 2018 Dec 1; 9(1). https://doi.org/10.1038/s41467-018-05077-9 PMID: 29985392

66. Murao A, Aziz M, Wang H, Brenner M, Wang P. Release mechanisms of major DAMPs. Apoptosis. 2021 Apr 1; 26(3–4):152–62. https://doi.org/10.1007/s10495-021-01663-3 PMID: 33713214

67. Cheng Y, Sun F, Wang L, Gao M, Xie Y, Sun Y, et al. Virus-induced p38 MAPK activation facilitates viral infection. Theranostics. 2020; 10(26):12223. https://doi.org/10.7150/thno.50992 PMID: 33204339

68. Wang L, Xia Z, Tang W, Sun Y, Wu Y, Kwok HF, et al. p38 activation and viral infection. Expert Rev Mol Med. 2022 Jan 21; 24. https://doi.org/10.1017/erm.2021.29 PMID: 35060846

69. Cesaro T, Michiels T. Inhibition of PKR by Viruses. Front Microbiol. 2021 Oct; 12:3184. https://doi.org/10.3389/fmicb.2021.757238 PMID: 34759908

70. Rabouw HH, Langereis MA, Knaap RCM, Dalebout TJ, Canton J, Sola I, et al. Middle East Respiratory Coronavirus Accessory Protein 4a Inhibits PKR-Mediated Antiviral Stress Responses. PLoS Pathog. 2016 Oct 1; 12(10). https://doi.org/10.1371/journal.ppat.1005982 PMID: 27783669

71. Melia CE, van der Schaar HM, Lyoo H, Limpens RWAL, Feng Q, Wahedi M, et al. Escaping Host Factor PI4KB Inhibition: Enterovirus Genomic RNA Replication in the Absence of Replication Organelles. Cell Rep. 2017 Oct 17; 21(3):587–99. https://doi.org/10.1016/j.celrep.2017.09.068 PMID: 29045829

72. Duke GM, Palmenberg AC. Cloning and synthesis of infectious cardiovirus RNAs containing short, discrete poly(C) tracts. J Virol. 1989; 63(4):1822–6. https://doi.org/10.1128/JVI.63.4.1822-1826.1989 PMID: 2538661

73. Zoll J, Hulshof SE, Lanke K, Lunel FV, Melchers WJG, Schoondermark-Van De Ven E, et al. Saffold Virus, a Human Theiler's-Like Cardiovirus, Is Ubiquitous and Causes Infection Early in Life. PLoS Pathog. 2009 May; 5(5). https://doi.org/10.1371/JOURNAL.PPAT.1000416 PMID: 19412527

74. Wessels E, Duijsings D, Notebaart RA, Melchers WJG, Kuppeveld FJM van. A Proline-Rich Region in the Coxsackievirus 3A Protein Is Required for the Protein To Inhibit Endoplasmic Reticulum-to-Golgi Transport. J Virol. 2005 Apr 15; 79(8):5163. https://doi.org/10.1128/JVI.79.8.5163-5173.2005 PMID: 15795300

75. Sorgeloos F, Jha BK, Silverman RH, Michiels T. Evasion of antiviral innate immunity by Theiler's virus L* protein through direct inhibition of RNase L. PLoS Pathog. 2013 Jun; 9(6). https://doi.org/10.1371/journal.ppat.1003474 PMID: 23825954